Single-component white light emitting $CdSe_xS_y$ alloy nanocrystals through phosphine-free route

Shilpi Jaiswal,[#] Jyotsana Pathak[#] and Abhijit Patra*

Semiconductor nanocrystals are promising for display and lighting devices. Herein, we report a facile one-pot synthetic route to fabricate white light emitting $CdSe_xS_y$ nanocrystals with enhanced quantum yield using CdO, S powder, and Se powder as precursors. The phosphine-free route was adopted, employing paraffin oil as the reducing agent and solvent for the fabrication. The optical properties can be effectively tailored by controlling the reaction time and the molar ratio of Se/S. The emission of pristine $CdSe_xS_y$ nanocrystals covered a broad visible range from 400 to 750 nm. The $CdSe_xS_y$ nanocrystals (Se/S = 0.4) exhibited white-light emission with quantum yield of 50 ± 3 % and Commission Internationale de l'Eclairage (CIE) chromaticity coordinates of (0.30, 0.31). The band-edge (~400-450 nm) to trap-state (~550-750 nm) emissions was tuned by controlling the Se/S ratio, and the different shades of white light were obtained. Furthermore, the quantum yield and CIE coordinates of the $CdSe_xS_y$ nanocrystals (Se/S = 0.4) were found to be similar even after 30 days of fabrication, showing the high stability of nanocrystals. The white light emission was retained in nanocrystals-embedded poly(methyl methacrylate) (PMMA) thin film and also in the hydrogel matrix. The one-pot, low-cost, scalable fabrication of white light emitting $CdSe_xS_y$ nanocrystals demonstrated in the present study offers promising scope in the solid-state display applications.

Introduction

White light emitting (WLE) materials capture the attention of the scientific community for the last few decades due to the applications in artificial lighting and display devices.[1-5] Currently, incandescent bulbs and fluorescent lamps employing mercury vapour are used heavily for the lighting applications possessing an environmental concern. Surface passivated inorganic semiconductor nanocrystals have been emerged as a new technology platform with a potential to replace the commercially used lamps. CdS and CdSe-based nanocrystals have been explored extensively for cellular imaging/ labelling,[6,7] solar cell,[8,9] and light emitting devices.[10-12] The unique optoelectronic properties in these nanocrystals often arise due to the confinement of charge carriers.[13] Further, tunable emission in colloidal nanocrystals is significantly influenced by the composition of the constituents.[14] High molar absorption coefficient as well as photoluminescence quantum yield (PLQY) are added advantages of semiconductor nanocrystals. Thus, a considerable effort has been given for the fabrication of WLE materials based on semiconductor nanocrystals. However, the use of the toxic phosphine-based solvent and often tedious fabrication routes retard the wide-scale application. Hence, it is worthy of developing cost-effective and environmentally benign synthetic protocols for semiconductor nanocrystals for solid-state white light emission.

Several approaches have been adopted to produce WLE semiconductor nanocrystals.[15] Simple mixing of red, green and blue (RGB) emitting nanocrystals leads to white light emission.[16-18] The coating of red and green emitting nanocrystals on a blue emitting diode was reported to obtain desired WLE materials.[19,20] However, the color purity and the long-term stability are the prime concerns with WLE materials obtained through additive mixing. Multishell nanocrystals produce white light due to the combination of the complementary emission colors from distinct shells.[21-23] The transition metal ion-doped WLE nanocrystals were also reported.[24,25] Even though high PLQY is obtained, but the fabrication of multishell or doped nanocrystals may require delicate synthetic procedures involving several steps.[21,26] The fine-tuning of the band-edge exciton emission and a broad, deep trap-state emission in ultrasmall nanocrystals can be a facile alternative methodology to obtain white light emission. In this context, WLE 'magic-sized' CdSe nanocrystals,[27-29] and trap-rich CdS nanocrystals were reported.[21,30] The white light emission from these nanocrystals is due to the presence of multiple emitting states rather than the mixture of particle sizes. However, the PLQYs of the defect-induced trap-rich WLE nanocrystals are still not significant enough to be applied in the solid-state lighting.

The reports on one-pot fabrication and optical properties of ternary WLE nanocrystals are limited.[31,32] Addressing the cardinal objective of developing WLE nanocrystals with high quantum efficiency, we fabricated a series of CdSeS alloy nanocrystals in phosphine-free conditions. The composition of alloy nanocrystals drives the band-edge and trap states emission, leading to tunable optical properties. The cadmium oxide (CdO), sulphur and selenium powder were used as precursors. We employed non-toxic and highly stable paraffin oil as a solvent and reducing agent. Thus, the low-cost fabrication route, without using any exotic chemicals and solvents, like trioctylphosphine (TOP), trioctylphosphine oxide (TOPO), tributylphosphine (TBP), and octadecene (ODE), is highly scalable. Additionally, the synthetic process does not require glove-box and high vacuum instruments. The one-pot fabrication of ternary $CdSe_xS_y$ nanocrystals with single-component white light emission through phosphine-free route, to the best of our knowledge, has not been explored. Moreover, we demonstrated the solid-state white light emission in nanocrystals embedded polymer thin film and hydrogel matrix.

Department of Chemistry, Indian Institute of Science Education and Research Bhopal, Bhopal Bypass Road, Bhauri, Bhopal 462066, Madhya Pradesh, India
E-mail: abhijit@iiserb.ac.in
[#]These authors contributed equally

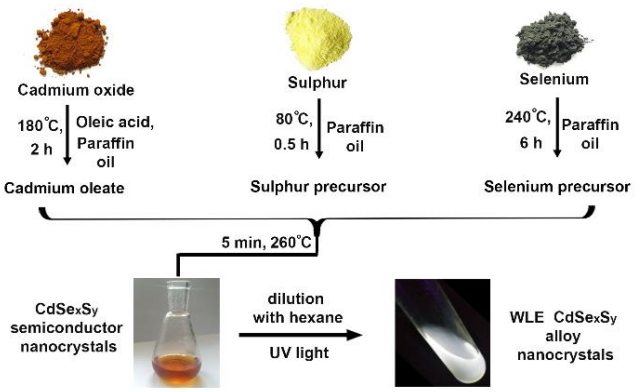

Scheme 1 Schematic illustrations for the synthesis of white light emitting (WLE) $CdSe_xS_y$ alloy nanocrystals.

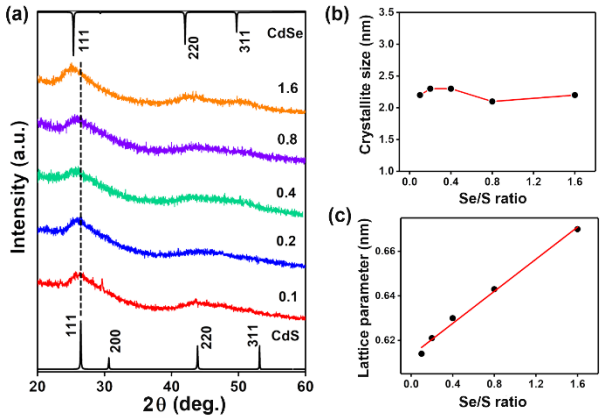

Fig. 1 (a) The powder X-ray diffraction (PXRD) patterns of $CdSe_xS_y$ nanocrystals at different Se/S molar ratio of 0.1 (red), 0.2 (blue), 0.4 (green), 0.8 (purple), and 1.6 (orange). The PXRD patterns of bulk CdS and CdSe are also shown. (b) The size of the nanocrystals calculated from the Scherrer equation as a function of Se/S ratio. (c) The linear relationship of the lattice parameters of $CdSe_xS_y$ nanocrystals as a function of Se/S molar ratio demonstrating the formation of homogeneous alloy nanocrystals.

Results and discussion

In an attempt to fabricate ternary alloy nanocrystals through phosphine-free route, we employed paraffin oil, oleic acid, CdO, Se, and S powder (Scheme 1). Deng et al. reported that Se could be dissolved in paraffin oil at 220 °C (melting point of Se in paraffin) to generate H_2Se, and that reacted with cadmium oleate to form CdSe nanocrystals.[33] Similarly, Yordanov et al. showed that the heating of S powder in paraffin oil resulted in the formation of H_2S, which upon reacting with cadmium oleate, led to the formation of CdS nanocrystals.[34] Herein, we used a similar strategy with modifications to fabricate ternary alloy $CdSe_xS_y$ nanocrystals. The reaction between CdO and oleic acid at 180°C yielded a cadmium oleate complex.[35] Se and S powder served as oxidising agents. H_2Se and H_2S were formed upon heating Se and S powder in paraffin oil, respectively, at 240 °C and 80 °C.[33, 34] The long-saturated hydrocarbon chain of paraffin oil was converted to the corresponding alkene. The FTIR spectra peaks at 1650 cm^{-1} obtained after heating Se or S with paraffin oil are attributed to C=C stretching. Finally, the reaction of cadmium oleate complex with H_2Se and H_2S led to the formation of $CdSe_xS_y$ ternary nanocrystals. The fabrication of the nanocrystals depends on factors such as temperature, time, and the molar concentration of the precursor.

Structural properties

The powder X-ray diffraction (PXRD) patterns of the alloy $CdSe_xS_y$ nanocrystals of different composition is shown in Fig. 1a. The PXRD patterns of the nanocrystals show a characteristic zinc-blende cubic structure with the planes at (111), (220) and (311).[36] The peak positions of $CdSe_xS_y$ nanocrystals of different Se/S ratios are compared with the bulk cubic CdSe and CdS. The diffraction peaks shift to lower Bragg's angle with the increase in the Se/S ratio (Fig. 1a). The continuous peak shift in the nanocrystals may also rule out the phase separation or separated nucleation of CdS or CdSe nanocrystals.[37] The broadening of diffraction peaks is due to the nano-sized dimension of the crystals.[37] The diffraction angles at (220) and (311), were also shifted. However, those peaks were less pronounced due to the ultra-small size of the nanocrystals. The average crystallite size was calculated using the Scherrer formula.[38] Accordingly, from the FWHM (full width at half maximum) of the (111) diffraction peak, it was found that $CdSe_xS_y$ nanocrystals were within the range of 2.1 ± 0.3 nm (Fig. 1b). Further, the lattice parameters were calculated from the PXRD patterns for different compositions of $CdSe_xS_y$ nanocrystals. As per the Vegard's law, the gradual increase in the lattice parameter with the increase in Se/S ratio in a linear fashion ascertains the formation of homogenous alloy nanocrystals (Fig. 1c).[39]

The size distribution and morphology of the $CdSe_xS_y$ nanocrystals were further corroborated through transmission electron microscopy (TEM). Fig. 2a depicts the particle size distribution of $CdSe_xS_y$ nanocrystals with Se/S = 0.4. Nearly monodispersed spherical particles with an average diameter of 2.4 ± 0.3 nm were obtained (Fig. 2b). The average particle size was found to be similar to the variation of Se/S composition. The energy dispersive X-ray (EDX) mapping using TEM revealed a homogeneous distribution of constituent elements in $CdSe_xS_y$ nanocrystals. The atomic percentage composition of Cd, Se, S in $CdSe_xS_y$ (Se/S = 0.4) was obtained through EDX spectroscopy. The lattice fringes and selected area electron diffraction (SAED) pattern further confirm the crystalline phase of nanocrystals (Fig. 2a).

Composition-dependent optical properties

The change in the molar ratio of Se and S in $CdSe_xS_y$ nanocrystals affects not only the structure but also the optical properties of the resulting nanocrystals.[40,41] The optical properties of semiconductor nanocrystals are largely dependent on particle size and distribution.[42] However, the optical properties of ternary nanocrystals can be tuned by varying the molar composition of the constituents.[40,43] The absorption spectra of the dispersion of $CdSe_xS_y$ nanocrystals in hexane with the different compositions are shown in Fig. 3a. The clear change in the absorption spectra of nanocrystals was observed with the increase of the Se content. Even though the particle size distribution remains similar, the variation in absorption spectra is due to the change in the composition of the nanocrystals.[44,45] The optical band gaps of the nanocrystals are obtained from the Tauc plot (Fig. 3b). The band gap energy of bulk CdSe is 1.74 eV, and that of CdS is 2.43 eV.[40] The band gap energy of $CdSe_xS_y$ nanocrystals was found to change nonlinearly with Se/S

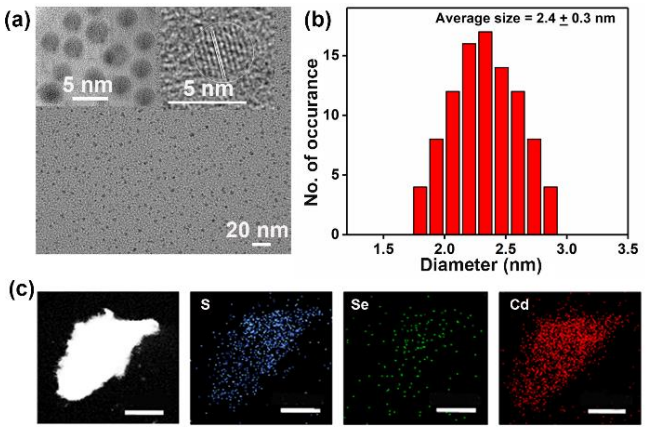

Fig. 2 (a) Transmission electron microscopy (TEM) image of $CdSe_xS_y$ nanocrystals (Se/S = 0.4); inset: magnified image of the nanocrystals and the fringe pattern. (b) The corresponding particle size distribution based on multiple images obtained from samples through different batches of synthesis, demonstrating the average particle size in the range of 2.4 ± 0.3 nm. (c) The energy-dispersive X-ray spectroscopy (EDS) mapping of the elemental distribution of S, Se, and Cd in $CdSe_xS_y$ nanocrystals using TEM; scale bar 500 nm.

composition (Fig. 3c). The nonlinear trend can be attributed to the following factors.[46,47] (i) The variation of lattice constant may change the band structure; (ii) the different electronegativities of atoms in the alloy nanocrystals deform the electronic distribution impacting the band structure. (iii) The fluctuation of the cation (Cd^{2+}) and anion (Se^{2-} or S^{2-}) bond lengths and bond angles for accommodating constituents of diverse ionic radii into a crystal lattice with the variation of composition is likely to affect the band structure.[46,47]

The normalized photoluminescence (PL) spectra of the $CdSe_xS_y$ nanocrystals dispersion in hexane are shown in Fig. 4a. Two emission peaks were observed for all the different compositions. The high and low energy peaks obtained upon exciting at 370 nm are attributed to the band-edge and the trap-state emission, respectively. The nanocrystals possess a wide emission range covering the whole visible spectrum. Whereas, the precursor materials do not show any photoluminescence. The PL spectra of $CdSe_xS_y$ nanocrystals were fitted into two Gaussian peaks. The narrow band-edge emission arises due to the direct recombination of the electron and hole within the nanocrystals.[48] The trap-state emission usually occurs when a photogenerated electron or holes are in a mid-gap state, and subsequently, relax to the ground state through radiative recombination.[49,50] A gradual red shift in PL was observed with the increasing molar ratio of Se in $CdSe_xS_y$ nanocrystals up to Se/S = 0.4 (Fig. 4a). The trend was reversed, and a blue shift in PL was observed on further incorporation of Se (for Se/S > 0.4). The analysis of PXRD and TEM images revealed a similar size distribution of $CdSe_xS_y$ nanocrystals with increasing Se concentrations. Hence, like the absorption spectra, the variation of emission characteristics of ternary nanocrystals is due to the change in composition.[45] The nonlinear trend in emission is presumably due to the variation of the band gap of ternary alloy nanocrystals compared to that of the pristine bulk semiconductor (CdS or CdSe).[40] Houtepen and coworkers assigned the nonlinear trend in absorption and PL spectra in In_xZn_yP nanocrystals with similar average particle size and different compositional ratios as the varied degree of quantum confinement that could be due to the change in the effective masses of electrons and holes in the alloy nanocrystals.[45] The similar quantum confinement effect could be another possible reason for the composition-dependent tunable optical properties of the $CdSe_xS_y$ nanocrystals (Se/S = 0.1 to 1.6).

The ratio of the trap-state to the band-edge emission increases with the increasing molar ratio of Se in $CdSe_xS_y$ nanocrystals. Thus, the PL of ternary alloy nanocrystals can easily be tuned by varying the composition.[31] The PL spectra of as-prepared nanocrystals (after 4 h) and after digestion for 5 days (Fig. 4a) were analysed. The ratio of the trap-state to the band-edge emission for the nanocrystals with higher Se percentage (Se/S > 0.4) decreased with the time of digestion at ambient temperature and became nearly constant after 3 days. However, the relative intensity of the band-edge and the trap-state emission remained similar with time for the nanocrystals with Se/S $\leq$ 0.4. The initial decrease of the trap-state emission compared to the band-edge with a higher percentage of Se might be due to the effect of composition and digestion time. [51,52] The Commission Internationale de l'Eclairage (CIE) chromaticity coordinates for nanocrystals of diverse compositions, and digestion time revealed different shades of white light (Fig. 4b). The CIE coordinates of $CdSe_xS_y$ nanocrystals of Se/S = 0.4 was found be (0.30, 0.31), very close to that of pure white light (0.33, 0.33).[53,54] The highest photoluminescence quantum yield (PLQY) of 50 ± 3 % was obtained for $CdSe_xS_y$ alloy nanocrystals with Se/S = 0.4 (Fig. 4c). The emission spectra and CIE coordinates

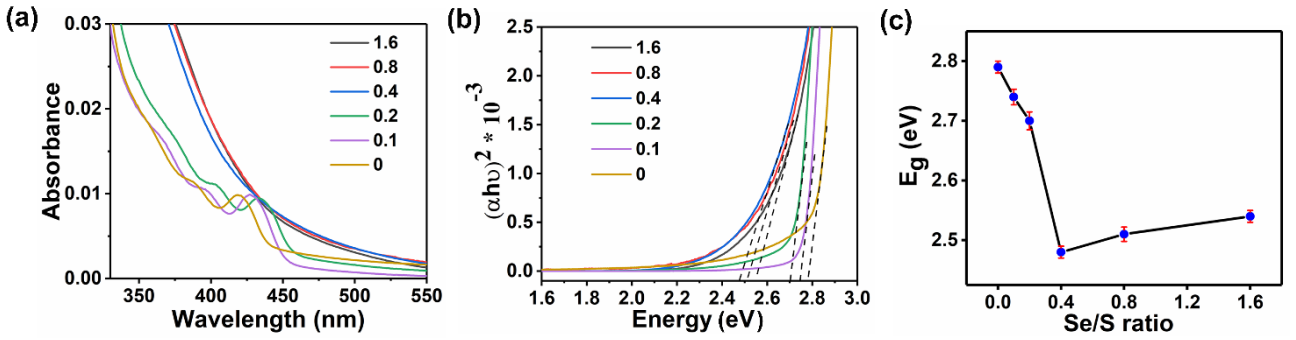

Fig. 3 (a) Absorption spectra of $CdSe_xS_y$ nanocrystals at a molar ratio of Se/S ranging from 0, 0.1, 0.2, 0.4, 0.8, to 1.6, dispersed in hexane; (b) Tauc plots for the corresponding nanocrystals; (c) estimation of the band gap energy using the Tauc method for $CdSe_xS_y$ nanocrystals with increasing Se/S ratio; the bars represent the standard deviation of triplicate measurements.

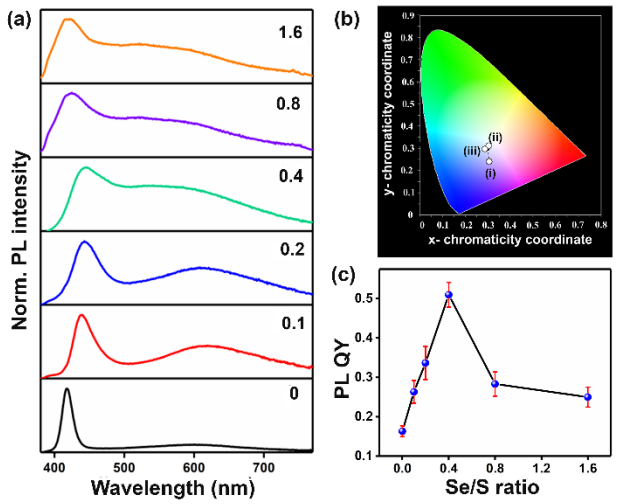

Fig. 4 Normalized emission spectra (λ_{exc} = 370 nm) of digested $CdSe_xS_y$ nanocrystals with variable Se/S ratio (0 – 1.6). (b) CIE chromaticity diagram of $CdSe_xS_y$ nanocrystals with Se/S ratio (i) 0.1, (ii) 0.4 and (iii) 1.6. (c) Photoluminescence quantum yield (PLQY) of $CdSe_xS_y$ nanocrystals as a function of the Se/S molar ratio; the bars represent the standard deviation of triplicate measurements.

of the $CdSe_xS_y$ nanocrystals (Se/S = 0.4) at different excitation wavelengths were found to be similar.

We have carried out time-correlated single photon counting (TCPSC) measurements to understand the origin of the band-edge and trap-state emission in $CdSe_xS_y$ nanocrystals. The emission decays of the nanocrystals were monitored at the shorter wavelengths (band-edge, 420-450 nm) and longer wavelengths (trap-state, 540-620 nm) for Se/S = 0.2, 0.4, 0.8. All the samples exhibit tri-exponential decays, which is in agreement with the previously reported literature.[55,56] The tri-exponential decay kinetics involves possible recombination pathways, band-edge, trap-states emission, and the electron/hole-trapping process. The ultrafast component suggests the electron or hole trapping process.[55] The fitted PL decay data for different alloy nanocrystals were analysed. The faster decay time is expected for band-edge emission than that of the trap-state.[48,57] The highest average decay time of 18.4 ns (band-edge, λ_{em} = 450 nm) and 29.8 ns (trap-state, λ_{em} = 560 nm) was observed for $CdSe_xS_y$ (Se/S = 0.4) nanocrystals. The mechanism for the band-edge and the trap-state emission in $CdSe_xS_y$ nanocrystals is schematically illustrated in Fig. 5. Upon photoexcitation, the band at higher energy arises due to the radiative recombination of band-edge excitons. Electrons transit from the conduction band to the trap state, originated due to the surface defect of the nanocrystals, subsequently, relax to the valence band leading to lower energy trap-state emission.

Furthermore, to study the growth mechanism of nanocrystals, we investigated the effect of reaction time on the optical properties of resultant $CdSe_xS_y$ nanocrystals with Se/S = 0.4 at a constant temperature of 260 °C. Only one emission peak was observed for the initial time of the reaction (1 min). The reaction was continued for 3 to 5 min. Subsequently, the two emission peaks were observed, attributed to the band-edge and the trap-state emission. The single-component white light emission in the nanocrystals is due to both band-edge and trap-state emission covering the whole visible spectrum. Further, the increase of the reaction time (7 to 10 min) resulted in the shift of the emission peak at the longer wavelength region with a significant decrease of the trap-state emission. The red-shift in the peak position, along with the spectral change is due to the continuous growth of the $CdSe_xS_y$ nanocrystals with increasing reaction time.[58] The contribution of the trap-state emission decreases with an increase in the size of nanocrystals, as the surface to volume ratio decreases.[48] The size and morphological analysis of the $CdSe_xS_y$ (Se/S = 0.4) nanocrystals obtained at a longer reaction time was carried out using TEM. The nanocrystals were spherical in shape, with a larger average particle size of 4.2 ± 0.3 nm. We have further carried out experiments for the fabrication of $CdSe_xS_y$ nanocrystals at a lower temperature, 220 °C and at a higher temperature, 300 °C. The white light emission from the as-prepared dispersion was not observed by varying the reaction temperature. Thus, controlling the reaction time, reaction temperature, and molar ratio of the precursor is essential for generating the white light-emitting semiconductor nanocrystals.

The stability of the nanocrystals is a critical issue that needs to be addressed for practical applications. It has been observed that the shell is wrapped on the core of the nanocrystals to improve the luminous efficiency and stability.[21] However, the shell often reduces the trap-states, leading to impaired white emission.[58] Moreover, the PLQY and the stability of the nanocrystals can also be improved by tuning the composition, reaction temperature, and time.[27,32,58] In the present case, the PLQY and the quality of white light were also improved by tuning the composition and fabrication conditions of the $CdSe_xS_y$ nanocrystals. The photoluminescence spectra of $CdSe_xS_y$ nanocrystals (Se/S = 0.4, reaction temperature: 260°C, reaction time: 5 min) were recorded after 30 days of digestion in hexane. The peak positions for the band-edge and the trap-state emission remain the same, and PLQY was found to be 43 - 45 % after 30 days of fabrication. The CIE coordinates of white light emission obtained from the dispersion after 4 days and 30 days of digestion were found to be similar (0.30, 0.31). Thus, the developed system is stable under ambient conditions.

White light emitting gel and thin film

The trap-state induced strong white light emission using phosphine-free solvent, promises potential applications for display and lighting

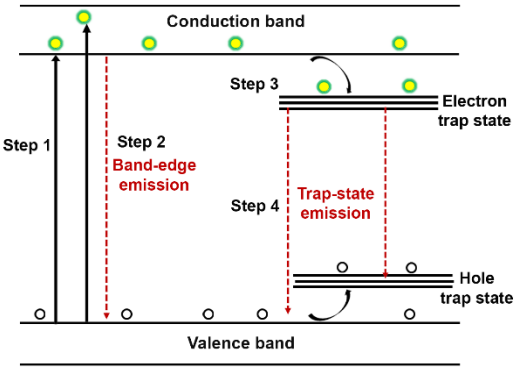

Fig. 5 Schematic illustration of the photoluminescence process in $CdSe_xS_y$ nanocrystals. Upon photoexcitation, electrons move from the valence band (VB) to the conduction band (CB) (step 1). The radiative recombination of band-edge excitons (recombination of CB electrons and VB holes, step 2). Few electrons transit from the conduction band to the trap state originated due to the surface defect of the nanocrystals (step 3). The radiative transition of electrons from the trap state leads to lower energy emission (step 4).

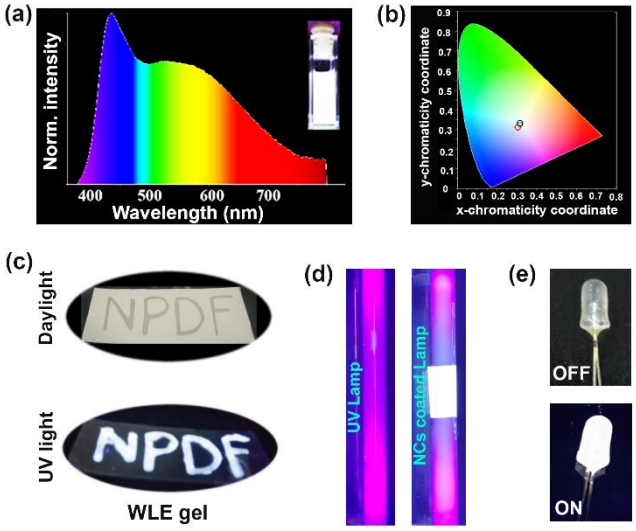

Fig. 6 (a) Emission spectrum of WLE $CdSe_xS_y$ (Se/S = 0.4) alloy nanocrystals dispersion in hexane; inset: the photographs of WLE dispersion. (b) CIE chromaticity diagram of WLE dispersion (0.30, 0.31; red), gel (0.31, 0.32; black) and thin film (0.31, 0.33; green). (c) Photographs of the script written using the WLE gel on a nonfluorescent silica plate under the illumination of daylight and UV light at 365 nm. (d) Photographs of normal UV lamp and the same wrapped in nanocrystals embedded poly(methyl methacrylate) (PMMA) thin film under the illumination of UV light at 365 nm. (e) Photographs of commercial light-emitting diode (LED) coated with $CdSe_xS_y$ nanocrystals embedded PMMA thin film under daylight (OFF) and UV light at 365 nm (ON).

devices. However, it is challenging to maintain the quality of white light upon assembling WLE $CdSe_xS_y$ nanocrystals in a gel or a polymer matrix. $CdSe_xS_y$ (Se/S = 0.4) nanocrystals were employed for the fabrication of WLE thin film due to the high quantum yield. 2 wt% of gelatin in 1 mL water was heated at 50°C and then was mixed with 1 mL dispersion of WLE $CdSe_xS_y$ (Se/S = 0.4) nanocrystals and 1 mL of acetone. The emission spectrum of the resulting WLE gel showed characteristic band-edge and trap-state emission as that of the WLE dispersion (Fig. 5a, S11a, ESI†). The CIE chromaticity coordinates of the white light obtained from the gel were found to be (0.31, 0.32), as shown in Fig. 6b. The color rendering index (CRI) and correlated color temperature (CCT) are useful parameters to judge the quality of white light in addition to CIE coordinates.[1,54,59] The CRI and CCT values of WLE gel were 74 and 6438 K, respectively. The non-fluorescent silica plate was further coated with the WLE gel, and the desired inscription (NPDF) could be written. The WLE gel showed a bright illumination when exposed to the UV light at 365 nm (Fig. 6c).

In order to explore the practical application in solid-state displays, poly(methyl methacrylate) (PMMA) was employed for the fabrication of homogeneous WLE thin film. 1.5 mL of 0.5 wt% PMMA solution in dichloromethane was mixed with 1.5 mL dispersion of WLE $CdSe_xS_y$ (Se/S = 0.4) nanocrystals. The emission spectrum of WLE thin film showed the characteristic band-edge and trap-state emission peaks as that of the WLE dispersion (Fig. 6a). The CIE chromaticity coordinates of the white light obtained from the thin film were found to be (0.31, 0.33), very close to that of pure white light (Fig. 6b). The CRI and CCT values of WLE thin film were 95 and 6453 K, respectively. The materials with CRI values range from 80 to 100, and CCT values within 2,500 to 7,500 K are considered for white light emitting devices.[60,61] Thus, CRI and CCT values obtained for $CdSe_xS_y$ nanocrystals embedded PMMA thin films are promising for solid-state lighting devices. Bright white light emission was observed when the thin film coated on a quartz plate was illuminated under UV light at 365 nm. The PL spectra of the thin film was found to be identical when excited at the different positions of the film. The result demonstrates the formation of a homogeneous and optically transparent thin film. Furthermore, the nanocrystals embedded PMMA thin film was coated on a UV lamp (Fig. 6d) and the commercially available light emitting diode (LED, Fig. 6e). Strong white light emission was demonstrated upon excitation.

Conclusions

We developed a convenient protocol for the fabrication of white light emitting $CdSe_xS_y$ ternary alloy nanocrystals. The optical properties of the nanocrystals were tuned by varying the Se/S ratio. The variation of the band-edge and the trap-state emission with the composition of alloy nanocrystals, resulted in the generation of white light emission. The developed protocol offers multiple advantages for the large-scale, cost-effective fabrication of the alloy nanocrystals without the use of inert atmosphere, high vacuum, or exotic chemicals. We expect that the alloying method demonstrated in this study can also be extended for the fabrication of high-quality alloy nanocrystals from other semiconductor materials. The stable white light emission was also demonstrated in the solid-state employing $CdSe_xS_y$ nanocrystals in the polymer thin film and hydrogel matrix. Such semiconductor alloy nanocrystals can be potential nano-emitters in the light emitting devices and promising as biological labels.

Experimental section

Characterization of Alloyed NCs

The average size of semiconductor nanocrystals was estimated from TEM using the FEI TALOS 200S instrument at a working voltage of 200 kV. The powder X-ray diffraction patterns were obtained using a PANalytical, Empyrean X-ray diffractometer with Cu Kα radiation (λ = 1.5418 Å). A Cary 100 spectrophotometer was used to examine the absorption spectra of the nanocrystals using 10 mm path length quartz cuvettes. The optical density of the dispersion of nanocrystals in hexane was maintained low (< 0.1) to rule out the possibility of the inner filter effect. A Jobin Yvon Horiba Model Fluorolog-3-21 was employed to measure the fluorescence spectra of nanocrystals. The quantum yields of the nanocrystals were estimated by the relative method comparing with a fluorescence standard. Time-resolved fluorescence measurements were carried out using time-correlated single photon counting (TCSPC) spectrometer (Delta Flex-01-DD/HORIBA). For recording instrument response function, we used an aqueous dispersion of colloidal silica (LUDOX). All samples were excited with diode lasers at 370 nm. All decay curves were examined by nonlinear least-squares iteration using IBH DAS6 (version 6.8) decay analysis software. The quality of the fit was evaluated by the fitting parameters (χ^2), and the visual inspection of the residuals. The decay time of nanocrystals was obtained from the decay curves, fitted using

multiexponetial model. CIE color coordinates, color rendering index (CRI), and correlated color temperature (CCT) values were obtained using Osram Sylvania (Color Calculator, version 6.31) software.

Conflicts of interest

There is no conflict to declare.

Acknowledgements

JP gratefully thanks DST-SERB, New Delhi, for the National Post-Doctoral Fellowship (N-PDF) award (PDF/2017/002426). SJ thanks IISERB and CSIR for the fellowship. Financial support from Council of Scientific and Industrial Research (CSIR), New Delhi, (No. 01(2878)/17/EMR-II), infrastructural support from IISERB, and the FIST-supported TEM facility to the Department of Chemistry, IISERB, is gratefully acknowledged. We thank Arkaprabha Giri and Subhankar Kundu for fruitful discussion and providing support in some of the experiments.

Notes and references

1. G. M. Farinola and R. Ragni, *Chem. Soc. Rev.*, 2011, **40**, 3467-3482.
2. N. J. Findlay, J. Bruckbauer, A. R. Inigo, B. Breig, S. Arumugam, D. J. Wallis, R. W. Martin and P. J. Skabara, *Adv. Mater.*, 2014, **26**, 7290-7294.
3. S. Das, T. Debnath, A. Basu, D. Ghosh, A. K. Das, G. A. Baker and A. Patra, *Chem. Eur. J.*, 2016, **22**, 8855-8863.
4. T. S. Mahapatra, H. Singh, A. Maity, A. Dey, S. K. Pramanik, E. Suresh and A. Das, *J. Mater. Chem. C*, 2018, **6**, 9756-9766.
5. S. Kundu, B. Sk, P. Pallavi, A. Giri and A. Patra, *Chem. Eur. J.*, 2020, **26**, 5557-5582.
6. J. K. Jaiswal and S. M. Simon, *Trends in Cell Biology*, 2004, **14**, 497-504.
7. S. Santra, H. Yang, P. H. Holloway, J. T. Stanley and R. A. Mericle, *J. Am. Chem. Soc.*, 2005, **127**, 1656-1657.
8. Y. L. Lee, B. M. Huang and H. T. Chien, *Chem. Mater.*, 2008, **20**, 6903-6905.
9. Y. Zhang, G. Wu, F. Liu, C. Ding, Z. Zou and Q. Shen, *Chem. Soc. Rev.*, 2020, **49**, 49-84.
10. S. Coe, W. K. Woo, M. Bawendi and V. Bulović, *Nature*, 2002, **420**, 800-803.
11. S. Bhandari, D. Mondal, S. K. Nataraj and R. G. Balakrishna, *Nanoscale Adv.*, 2019, **1**, 913-936.
12. E. Jang, S. Jun, H. Jang, J. Lim, B. Kim and Y. Kim, *Adv. Mater.*, 2010, **22**, 3076-3080.
13. C. B. Murray, D. J. Norris and M. G. Bawendi, *J. Am. Chem. Soc.*, 1993, **115**, 8706-8715.
14. T. Aubert, M. Cirillo, S. Flamee, R. V. Deun, H. Lange, C. Thomsen and Z. Hens, *Chem. Mater.*, 2013, **25**, 2388-2390.
15. Q. Dai, C. E. Duty and M. Z. Hu, *Small*, 2010, **6**, 1577-1588.
16. R. Boonsin, A. Barros, F. Donat, D. Boyer, G. Chadeyron, R. Schneider, P. Boutinaud and R. Mahiou, *ACS Photonics*, 2018, **5**, 462-470.
17. S. Dai, C. B. Siao, S. R. Chung, K. Wang and X. Pan, *J. Mater. Chem. C*, 2018, **6**, 3089-3096.
18. Y. Q. Li, A. Rizzo, R. Cingolani and G. Gigli, *Adv. Mater.*, 2006, **18**, 2545-2548.
19. J. Cho, Y. K. Jung, J. K. Lee and H.S. Jung, *Langmuir*, 2017, **33**, 13040-13050.
20 B. Chen, H. Zhong, M. Wang, R. Liu and B. Zou, *Nanoscale*, 2013, **5**, 3514-3519.
21. S. Sapra, S. Mayilo, T. A. Klar, A. L. Rogach and J. Feldmann, *Adv. Mater.*, 2007, **19**, 569-572.
22. D. Y. Jo and H. Yang, *Chem. Commun.*, 2016, **52**, 709-712.
23. S. Pramanik, S. Bhandari and A. Chattopadhyay, *J. Mater. Chem. C*, 2017, **5**, 7291-7296.
24. S. K. Panda, S. G. Hickey, H. V. Demir and A. Eychmüller, *Angew. Chem. Int. Ed.*, 2011, **50**, 4432-4436.
25. W. J. Zhang, C. Y. Pan, F. Cao and X. Yang, *J. Mater. Chem. C*, 2017, **5**, 10533-10542.
26. C. Liao, L. Tang, X. Gao, R. Xu, H. Zhang, Y. Yu, C. Lu, Y. Cui and J. Zhang, *Nanoscale*, 2015, **7**, 20607-20613.
27. M. J. Bowers, J. R. McBride and S. J. Rosenthal, *J. Am. Chem. Soc.*, 2005, **127**, 15378-15379.
28. T. G. Mack, L. Jethi and P. Kambhampati, *ACS Photonics*, 2019, **6**, 1118-1124.
29. Y. Wang, Y. H. Liu, Y. Zhang, F. Wang, P. J. Kowalski, H. W. Rohrs, R. A. Loomis, M. L. Gross and W. E. Buhro, *Angew. Chem. Int. Ed.*, 2012, **51**, 6154-6157.
30. A. Veamatahau, B. Jiang, T. Seifert, S. Makuta, K. Latham, M. Kanehara, T. Teranishi and Y. Tachibana, *Phys. Chem. Chem. Phys.*, 2015, **17**, 2850-2858.
31. H. S. Chen, S. R. Chung, T. Y. Chen and K. Wang, *J. Mater. Chem. C*, 2014, **2**, 2664-2667.
32. Y. C. Chen, H. S. Chen, S. R. Chung, J. K. Chang and K. Wang, *J. Mater. Chem. C*, 2015, **3**, 5881-5884.
33. Z. Deng, L. Cao, F. Tang and B. Zou, *J. Phys. Chem. B*, 2005, **109**, 16671-16675.
34. G. G. Yordanov, H. Yoshimura and C. D. Dushkin, *Colloid Polym. Sci.*, 2008, **286**, 813-817.
35. N. Grumbach, R. K. Capek, E. Tilchin, A. Rubin-Brusilovski, J. Yang, Y. Ein-Eli and E. Lifshitz, *J. Phys. Chem. C*, 2015, **119**, 12749-12756.
36. C. Ünlü, G. Ü. Tosun, S. Sevim and S. Özçelik, *J. Mater. Chem. C*, 2013, **1**, 3026-3034.
37. X. Zhong, Y. Feng, W. Knoll and M. Han, *J. Am. Chem. Soc.*, 2003, **125**, 13559-13563.
38. A. L. Patterson, *Phys. Rev.*, 1939, **56**, 978-982.
39. V. Tallapally, T. A. Nakagawara, D. O. Demchenko, Ü. Özgür and I. U. Arachchige, *Nanoscale*, 2018, **10**, 20296-20305.
40. D. Yu, K. Du, J. Zhang, F. Wang, L. Chen, M. Zhao, J. Bian, Y. Feng and Y. Jiao, *New J. Chem.*, 2014, **38**, 5081-5086.
41. L. Y. Chen, P. A. Yang, C. H. Tseng, B. J. Hwang and C. H. Chen, *Appl. Phys. Lett.*, 2012, **100**, 163113.
42. I. S. Sohn, S. Unithrattil and W. B. Im, *ACS Appl. Mater. Interfaces*, 2014, **6**, 5744-5748.
43. B. Xing, W. Li, X. Wang, H. Dou, L. Wang, K. Sun, X. He, J. Han, H. Xiao, J. Miao and Y. Li, *J. Mater. Chem.*, 2010, **20**, 5664-5674.
44. R. Zhou, L. Wan, H. Niu, L. Yang, X. Mao, Q. Zhang, S. Miao, J. Xu and G. Cao, *Sol. Energy Mater. Sol. Cells*, 2016, **155**, 20-29.
45. F. Pietra, L. D. Trizio, A. W. Hoekstra, N. Renaud, M. Prato, F. C. Grozema, P. J. Baesjou, R. Koole, L. Manna and A. J. Houtepen, *ACS Nano*, 2016, **10**, 4754-4762.
46. I. Hadar, X. Hu, Z. Z. Luo, V. P. Dravid and M. G. Kanatzidis, *ACS Energy Lett.*, 2019, **4**, 2137-2143.
47. L. A. Swafford, L. A. Weigand, M. J. Bowers, J. R. McBride, J. L. Rapaport, T. L. Watt, S. K. Dixit, L. C. Feldman and S. J. Rosenthal, *J. Am. Chem. Soc.,* 2006, **128**, 12299-12306.
48. M. Abdellah, K. J. Karki, N. Lenngren, K. Zheng, T. Pascher, A. Yartsev and T. Pullerits, *J. Phys. Chem. C*, 2014, **118**, 21682-21686.

49. C. Giansante and I. Infante, *J. Phys. Chem. Lett.*, 2017, **8**, 5209-5215.
50. M. Jones, S. S. Lo and G. D. Scholes, *J. Phys. Chem. C*, 2009, **113**, 18632-18642.
51. S. Banerjee, B. G. Maddala, F. Ali and A. Datta, *Phys. Chem. Chem. Phys.*, 2019, **21**, 9512-9519.
52. J. Zhang, W. Sun, L. Yin, X. Miao and D. Zhang, *J. Mater. Chem. C*, 2014, **2**, 4812-4817.
53. Y. S. L. V. Narayana, S. Basak, M. Baumgarten, K. Müllen and R. Chandrasekar, *Adv. Funct. Mater.*, 2013, **23**, 5875-5880.
54. P. Pallavi, S. Bandyopadhyay, J. Louis, A. Deshmukh and A. Patra, *Chem. Commun.*, 2017, **53**, 1257-1260.
55. J. D. Keene, J. R. McBride, N. J. Orfield and S. J. Rosenthal, *ACS Nano*, 2014, 8, 10665-10673.
56. K. E. Knowles, E. A. McArthur and E. A. Weiss, *ACS Nano*, 2011, **5**, 2026-2035.
57. D. R. Baker and P. V. Kamat, *Langmuir,* 2010, **26**, 11272.
58. I. Fossé, S. Brinck, I. Infante, and A.J. Houtepen, *Chem. Mater.* 2019, **31**, 4575−4583.
59. S. Dai, Y. S. Su, S. R. Chung, K. Wang and X. Pan, *Nanoscale*, 2018, **10**, 10256-10261.
60. P. Pallavi, B. Sk, P. Ahir and A. Patra, *Chem. Eur. J.*, 2018, **24**, 1151-1158.
61. Y. Cui, T. Song, J. Yu, Y. Yang, Z. Wang and G. Qian, *Adv. Funct. Mater.*, 2015, **25**, 4796-4802.